

# Topological Effects of Noise on Nonlinear Dynamics

Gisela D. Charó,<sup>1,2,\*</sup> Mickaël D. Chekroun,<sup>3,4</sup> Denisse Sciamarella,<sup>2</sup> and Michael Ghil<sup>3,5</sup>

<sup>1</sup>*Centro de Investigaciones del Mar y la Atmósfera, Facultad de Ciencias Exactas y Naturales, Universidad de Buenos Aires, C1428EGA CABA, Argentina.*

<sup>2</sup>*Institut Franco-Argentin d'Études sur le Climat et ses Impacts (IFAEICI), UMI 3351 (CNRS-CONICET-UBA), C1428EGA CABA, Argentina.*

<sup>3</sup>*Department of Atmospheric & Oceanic Sciences, University of California, Los Angeles, CA 90095-1565, USA*

<sup>4</sup>*Weizmann Institute of Science, Rehovot, Israel.*

<sup>5</sup>*Geosciences Department and Laboratoire de Météorologie Dynamique (CNRS and IPSL), École Normale Supérieure and PSL University, 75231 Paris Cedex 05, France*

(Dated: October 30, 2020)

Noise modifies the behavior of chaotic systems. Algebraic topology sheds light on the most fundamental effects involved, as illustrated herein by using the Lorenz (1963) model. This model's attractor is “strange” but frozen in time. When driven by multiplicative noise, the Lorenz model's random attractor (LORA) evolves in time. Here, we use Branched Manifold Analysis through Homologies (BraMAH) to describe LORA's coarse-grained topology. BraMAH is thus extended from deterministic flows to noise-driven systems. LORA's homology groups change in time and differ from the deterministic one.

## I. INTRODUCTION

The climate system has a complex and nonlinear behavior, and its fundamental components — the atmosphere, oceans, and ice sheets — evolve on many different time and space scales [1, 2]. This unstable and dissipative system exhibits natural variability and is driven by external forcings [3, 4]. Physically open systems, modeled as dynamical systems with time-dependent forcing and coefficients, allow for deterministic as well as random forcing, due to both natural and anthropogenic causes.

The theory of nonautonomous (NDSs; [5]) and random (RDSs; [6]) dynamical systems provides the appropriate mathematical setting to address genuine interaction between intrinsic climate variability and its forced change in time [7]. The climate system's bifurcations [1] have gained further attention since the introduction of the term “tipping points” [8, 9]. The latter generalize, in fact, the bifurcation concept to open systems that are modeled by NDSs or RDSs [3, 4, 10].

In examples such as the ocean's wind-driven circulation [3, 7], a certain degree of realism requires considering not only a stochastic time-dependent forcing but also relying on a model's probability density function (PDF) rather than on pointwise simulation alone. The study of RDSs and their time-dependent invariant measures  $\mu_t$ , known as sample measures [11, 12], addresses these challenges [7, 13]; see Appendices A-C.

Algebraic topology [14] studies algebraic invariants that classify topological spaces up to homeomorphism [15]. Applications to deterministic dynamical systems are relatively recent and are also known as chaos topology [16–18]. Chaotic attractors can be classified by their branched manifolds [19, 20].

An approach to extract a branched manifold's topology from time series has been formulated [21] and applied to noisy data [22] and to material lines in fluid flows [23]. The approach, called Branched Manifold Analysis through Homologies (BraMAH), uses the latter to extract the topological structure of chaotic flows from data, i.e. from numerical or experimental time series produced by deterministically chaotic systems. The procedure requires (a) embedding the time series in a suitable phase space to obtain a multidimensional point cloud, and (b) approximating the structure of the branched manifold that supports the point cloud by a cell complex, as defined in algebraic topology [24]. These cells form a coarse-grained structure or “skeleton” of the branched manifold, whose topology can be algebraically calculated. Some of the branches may have torsions that are important for the correct identification of an attractor; hence BraMAH also distinguishes, for instance, a standard strip from a Möbius strip or a torus from a Klein bottle.

Topological Data Analysis (TDA) relies on recent computational advances, including homology computation from point clouds, to study the shape and structure of large data sets by focusing on the connectivity of the data [25–27]. TDA is used more and more in many research areas that are as diverse as image processing [28], the spread of social and biological contagions on networks [29], percolation theory [30], genomics and evolutionary dynamics [31, 32], protein structure [33], and so on.

Key developments in TDA include the computation of Persistence Homologies (PHs) [34, 35], which use a parameter to construct a family of nested cell complexes that monitor the “lifetime” of basic topological features in a point cloud, such as its holes. PHs were applied to shed further light on the strange attractor of the Lorenz system [36], among other well-known chaotic systems.

BraMAH [21–23] can be seen as a TDA method specifically designed to study chaotic attractors. The manner

---

\* gisela.charo@cima.fcen.uba.ar

in which BraMAH constructs the cell complex in a system’s phase space takes advantage of the fact that the point cloud under study must obey the property of lying on a branched manifold. This property is used to produce cell complexes in which each cell is representative of a large number of points that jointly approximate a locally Euclidean set.

The advantage of BraMAH is that one thus constructs a skeleton with just a few bones — as many as necessary but not many more — which (i) respects the local dimension of the manifold associated with the attractor, and (ii) whose topology is easy to extract, since the number of cells in the complex is much lower than the number of points in the original point cloud. Moreover, BraMAH goes well beyond just counting holes. Each hole in BraMAH identifies a branch of the manifold of interest, and it is expressed in terms of the points of the data cloud that were used to identify it. Hence, the user can distinguish the different branches and discern how they interconnect. In other words, BraMAH provides all the information needed to identify the attractor through its branched manifold: it is a TDA approach tailored for nonlinear dynamics.

The question that inevitably arises about random attractors is: what is the effect of a stochastic perturbation on a nonlinear system’s topological structure? Chekroun et al. [13] have shown that the well-known smoothing effect of noise disappears in a pullback approach. When the unperturbed nonlinear system’s dynamics is chaotic, the random pullback attractor is a time-dependent object that typically exhibits a fine structure of amazing complexity that is highlighted by its sample measure.

More precisely, random attractors demonstrate that fractal structures can survive the noise and be fed by it, as shown for the first time numerically in [13] for the stochastic Lorenz [37] model’s random attractor, dubbed LORA. This striking property arises, in particular, when the stochastic-dynamic system’s generator is hypoelliptic and its leading Lyapunov exponent is positive [13].

This paper presents, as far as we know, the first application of BraMAH to nonlinear, chaotic systems driven by noise. In it, we show that the random attractor’s structure is well represented, at each instant in time, by a branched manifold. The latter is defined here locally as an integer-dimensional subset of phase space that provides a robust skeleton of the point cloud associated with the sample measure; see Appendix C. This definition of a branched manifold is more general than the usual one in the purely deterministic context, where the invariant manifold is relative to a flow in phase space and defined through a Birman-Williams projection [17, 19].

The present work shows how the topological structure approximating LORA’s instantaneous sample measure is seen through the lens provided by the homological description of its associated branched manifold. We study here changes in LORA’s topology — *i.e.*, topological tipping points — produced by the driving noise.

## II. METHOD

Sciamarella and Mindlin [21, 22] formulated the BraMAH method and used it to extract the topological structure of chaotic flows from noisy time series. To do so, one embeds the time series in a suitable phase space of dimension  $n$  in order to generate a point cloud. Dynamically generated point clouds are well described by a branched manifold. The structure of this invariant manifold can be approximated with “building blocks.”

In algebraic topology, these building blocks are Euclidean closed sets (segments, disks, etc.), called  $n$ -cells, where  $n \in \mathbb{N}_0$ . A point is a 0-cell, a line segment joining two points is a 1-cell, a polygon is a 2-cell and so forth. Assembling these cells forms the cell complex that is the branched manifold’s skeleton.

The topological structure of this cell complex is studied by using the homology groups  $H_k$  [24] that identify the nonequivalent  $k$ -dimensional holes ( $k$ -holes) of a topological space of dimension  $n$ , where  $k \in \mathbb{N}_0$  and  $k \leq n$ . The group  $H_0$  identifies the connected components (0-holes),  $H_1$  the cycles (1-holes),  $H_2$  the cavities (2-holes), and  $H_n$  the hypercavities ( $n$ -holes).

When evaluating a time-dependent structure like LORA, one has to ask whether its topology is time-dependent. In order to answer this question, we will take two steps: (1) generate the point clouds that approximate LORA at successive time instants, called “snapshots” [13, 38, 39]; and (2) compute the topological properties associated with each snapshot using BraMAH.

In step (1), the point cloud approximating LORA is generated by solutions of the stochastic Lorenz model (SLM) introduced in [13]. In SLM, the equations of the classical Lorenz [37] deterministic model are perturbed by a multiplicative noise in the Itô sense [6], with  $W_t$  a Wiener process and  $\sigma > 0$  the noise intensity:

$$\begin{aligned} dx &= s(y - x)dt + \sigma x dW_t, \\ dy &= (rx - y - xz)dt + \sigma y dW_t, \\ dz &= (-bz + xy)dt + \sigma z dW_t; \end{aligned} \quad (1)$$

here  $r = 28$ ,  $s = 10$ ,  $b = 8/3$  are the standard parameter values for chaotic behavior.

The time-dependent sample measures  $\mu_t$  associated with the SLM system (1) are probability measures for the population density of any ensemble of initial data driven by the same noise realization until time  $t$ , after removal of the transient behavior. Mathematically, these measures are of Sinai-Ruelle-Bowen (SRB) type [12, 40, 41], *i.e.*, they are supported by the foliation of unstable manifolds that structure the random attractor [13].

A numerical estimation  $\hat{\mu}_t$  of such a measure can be computed at any time instant  $t$  by a pullback approach, *i.e.* by letting a large set of  $N_0$  initial points  $\{(x_j, y_j, z_j)(t = 0) : j = 1, \dots, N_0\}$  “flow” in phase space from the remote past until time  $t$ , for a fixed noise realization  $\omega$ . The convergence of the sample measure’s approximation  $\hat{\mu}_t = \hat{\mu}_t(N_0)$  is studied as the number  $N_0$  of

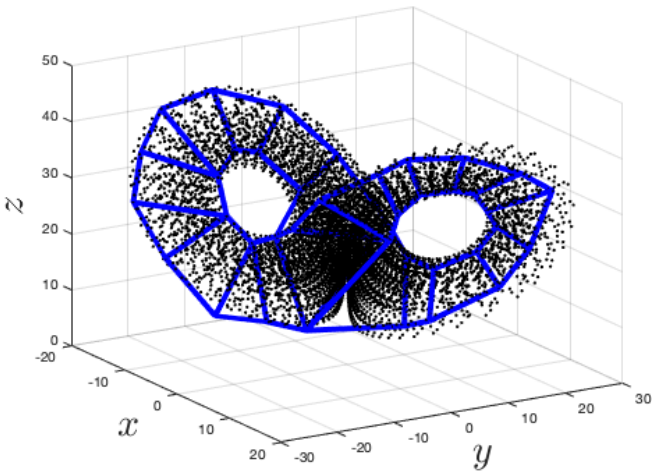


FIG. 1: Point cloud juxtaposed on the cell complex (blue lines) obtained by BraMAH for the deterministic Lorenz [37] attractor, with  $\sigma = 0$  in Eq. (1).

initial points increases; it is observed herein for  $N_0 \simeq 10^8$ .

Each point within a single point cloud at time  $t$  is mapped to a value of  $\hat{\mu}_t$  that is obtained by averaging over a volume surrounding that point: higher or lower  $\hat{\mu}_t$ -values correspond to more or less populated regions of the random attractor. We are interested in characterizing the topology of the point cloud's most populated regions but also in ascertaining this topology's robustness and persistence as  $N_0$  changes. In order to do this, a threshold  $\bar{n}$  for  $\hat{\mu}_t$  must be selected, as discussed later.

As stated in Sec. I, BraMAH computes the topology of a point cloud by assuming that points are locally distributed around a branched manifold. An  $m$ -branched manifold in  $n$  dimensions is a manifold with local dimension  $m$ ,  $m \leq n$ ;  $m = 2$  and  $n = 3$  in the case at hand.

One can thus approximate locally sets of points by  $m$ -disks. The points in the cloud are classified by “patch decomposition” into locally defined patches of points. This procedure ensures that each patch has points in common with the neighboring ones, in order to keep track of the gluing prescriptions between them.

Next, each patch will be associated with a cell. A  $k$ -cell is a set that is mapped through a continuous invertible map into the interior of a  $k$ -disk, with boundaries divided into a finite number of lower-dimensional cells, called faces. A cell complex  $\mathbb{K}_h$  of dimension  $h$  is a finite set of cells, such that their faces are elements of the complex, the interiors of no two cells intersect, and the highest dimensional cell is an  $h$ -cell. A  $k$ -chain is a linear combination of  $k$ -cells with integer coefficients. The algebra of these chains allows for a description of the connectivity of the cells at each  $k$ -level. A  $k$ -hole is a closed chain, called a  $k$ -cycle, that is not the border of any higher-dimensional cell.

Note that in BraMAH, the local dimension  $m$  of the branched manifold always matches the dimension  $h$  of the cell complex. Hence, in all the cases discussed herein,  $h = 2$  since  $m = 2$ . It is worth mentioning that most

TDA methods produce complexes that do not necessarily share this property and high-dimensional cells may be obtained even for 2-dimensional point clouds [34, 35].

The topological properties of the branched manifold associated with a cell complex  $\mathbb{K}_h$  are expressed in terms of the generators of its homology groups  $\{H_k : k = 0, \dots, h\}$  that identify the holes and of its orientability chains that represent the torsions. In order to compute the  $H_k$  groups, BraMAH builds a boundary matrix that uses the borders of the cells to determine which  $k$ -cycles are homologous to others. The  $k$ -cycles that are homologically independent are appended to  $H_k$ . The result is a set of homology groups  $H_k$  spelled out in terms of their generators, i.e., in terms of the explicit  $k$ -cycles representing them.

By construction, the BraMAH cell complex is uniformly oriented, with all the cells being assigned the same orientation. The integer multiples found in the chain that sums up all the  $k$ -borders of the complex are gathered in the orientability set  $\mathbb{O}_k$ . The elements in  $\mathbb{O}_1$  indicate the number and location of torsions that may be present in the 1-holes of the cell complex or not.

### III. RESULTS

To start our study, we provide first a BraMAH analysis of the classical Lorenz [37] attractor, with  $\sigma = 0$  in Eq. (1). The strange attractor and the cell complex associated with its 2-dimensional branched manifold is shown in Figure 1. The cell complex presents one connected component, i.e.,  $H_0 \sim \mathbb{Z}$ , and two homologically independent 1-holes associated with each wing of the butterfly, i.e.,  $H_1 \sim \mathbb{Z}^2$ ; there are no torsions, i.e.,  $\mathbb{O}_1 \sim \emptyset$ , and no enclosed cavities, i.e.,  $H_2 \sim \emptyset$ .

Generating point clouds associated with solutions of the SLM yields data sets in the form of 3-dimensional point clouds of  $N_0 = 10^8$  points. These point clouds are filtered, and the points in the filtered cloud correspond to  $\hat{\mu}_t$  values greater than a threshold value  $\bar{n}$ . These filtered point clouds are used to construct cell complexes at each  $\bar{n}$  value using the BraMAH method.

In Figure 2, LORA is computed at time  $t = 40.27$  with noise intensity  $\sigma = 0.3$ . The barplot in panel (a) shows the lifetime of 1-holes — i.e., of  $H_1$  generators — as the density threshold  $\bar{n}$  is increased: each bar starts at the first  $\bar{n}$ -value where the 1-hole appears, and ends at the  $\bar{n}$  where it disappears. Notice that, at this  $t$ -value, there are only four 1-holes that are “long-lived” as the value  $\bar{n}$  of the threshold increases.

The filtered point cloud is constructed using  $\bar{n} = 2 \times 10^{-4}$  as threshold value for the estimated sample measure  $\hat{\mu}_t$ : Figure 2(b) shows the projection of the filtered point cloud onto the  $(y, z)$ -plane, with thirteen 1-holes colored and three of them labeled with the numbers (1), (2) and (3). Panel (c) shows a 3-dimensional view of the filtered point cloud with the persistent 1-hole labeled with number (4) in red. The colors of the holes corre-

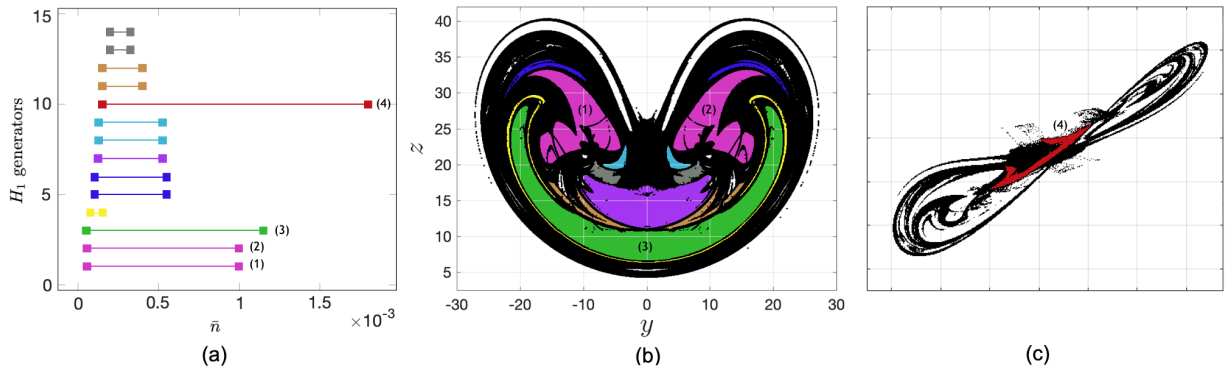


FIG. 2: LORA snapshot at  $t = 40.27$ , for  $\sigma = 0.3$ . (a) lifetime of the 1-holes as the density threshold  $\bar{n}$  is increased; the longest-lived ones are labeled with numbers (1)–(4); (b)  $(y, z)$  projection of the filtered point cloud ( $\bar{n} = 2 \times 10^{-4}$ ) with 13 colored 1-holes; (c) projection onto the plane  $-2.25x - 20y + 6z = 0$  of the filtered point cloud with the 1-hole labeled (4) in red.

spond to those of the bars in the barplot of Fig. 2(a). In this work, we analyze the topology of successive LORA snapshots with noise intensity  $\sigma = 0.3$ .

The local dimension of the branched manifold remains the same as in the deterministic case: LORA is thus a locally 2-branched manifold and no torsions are ever observed, i.e.,  $O_1 \sim \emptyset$ . Noise adds neither connected components nor cavities to the manifold, so that the groups  $H_0 \sim \mathbb{Z}$  and  $H_2 \sim \emptyset$  are the same as in Figure 1. The topological distinctions between LORA and the classical strange attractor of Lorenz [37] are thus solely present in  $H_1$ . One notices that the number of 1-holes changes from one snapshot to another, with holes created or destroyed by the noise in the course of time.

This situation is illustrated in Figure 3 for three successive snapshots, at  $t = 40.09, 40.18$  and  $40.27$ ; for each snapshot, we selected a threshold value  $\bar{n}$  at which the most persistent 1-holes occur. The filtered point clouds are given in the 3 top panels, while the corresponding cell complexes are presented in the 3 bottom panels. The number of 1-holes undergoes large changes from one snapshot to the next, as suggested by the video of LORA in the Supplementary Material of Chekroun et al. [13].

#### IV. CONCLUSION

We have presented here a topological analysis of a paradigmatic random attractor associated with the Lorenz convection model. The associated branched manifold provides a coarse-grained skeleton of this attractor.

Our study shows a marked difference between the unperturbed and the noise-driven cases. The stochastically perturbed system's random attractor, dubbed LORA, presents a much richer structure than the deterministic strange attractor, with a topology that also changes drastically in time. We believe that the framework introduced in this article to characterize such changes in topological features offers promising perspectives for the understanding of topological tipping points in general.

#### ACKNOWLEDGMENTS

This work is supported by the MATH-GEO (18-MATH-04) project of the Regional Program MATH-AmSud (D.S.). G.D.C. gratefully acknowledges support of her postdoctoral scholarship from CONICET and wishes to thank Juan Ruiz and the CIMA computing staff for support with the computations. M.D.C.'s work has been partially supported by the European Research Council (ERC) under the European Union's Horizon 2020 research and innovation program (Grant Agreement No. 810370). The article is TiPES contribution #46; this project has received funding from the European Union's Horizon 2020 research and innovation program under grant agreement No. 820970 (M.G.)

#### APPENDIX A: PULLBACK ATTRACTORS

We summarize herein some pertinent facts on nonautonomous systems of ordinary differential equations,

$$\dot{x} = F(t, x), \quad t \in \mathbb{R}, \quad (2)$$

considered in the framework of nonautonomous dynamical systems (NDSs);  $F$  denotes a smooth time-dependent vector field that governs the time evolution of the state  $x$  in a phase space  $X$ , taken for simplicity to be the Euclidean space  $\mathbb{R}^N$ .

Once existence and uniqueness are guaranteed, one can assign to this NDS a solution map  $\Phi(t, s)$ , which provides a two-time description of the motion: the time  $s$  when the system was initialized, and the time  $t \geq s$  of the system's current state. Thus

$$x(t) = \Phi(t, s)x_0$$

denotes the solution of Eq. (2) at time  $t$ , when initialized at  $x(t) = x_0$  for time  $t = s$ . In the autonomous case, only the time interval  $t' = t - s$  separating  $s$  and  $t$  matters and  $\Phi(t, s)$  reduces to a standard flow  $\Phi(t')$ .

In the case of forced and dissipative systems, such as the climate system [1, 4], one can define a collection of subsets called a *pullback attractor* (PBA) [6, 7, 13, 42, 43].



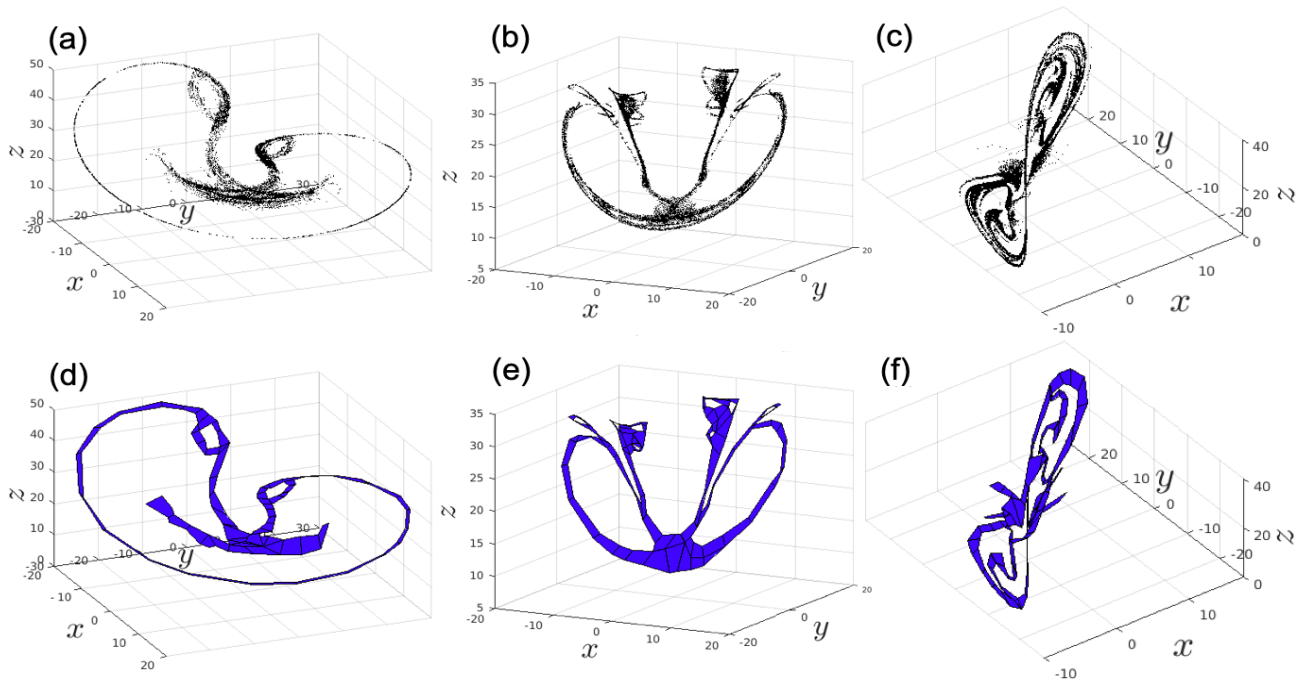


FIG. 3: Two representations of LORA snapshots with  $\sigma = 0.3$  and  $N_0 = 10^8$ : filtered point clouds (a)–(c) and cell complexes (d)–(f). (a,d)  $t = 40.09$ ,  $\bar{n} = 6 \times 10^{-4}$ ,  $H_1 \sim \mathbb{Z}^3$ ; (b,e)  $t = 40.18$ ,  $\bar{n} = 2.25 \times 10^{-3}$ ,  $H_1 \sim \mathbb{Z}^{10}$ ; and (c,f)  $t = 40.27$ ,  $\bar{n} = 7 \times 10^{-4}$ ,  $H_1 \sim \mathbb{Z}^4$ .

**Definition 1** A PBA is a family  $\bigcup_{t \in \mathbb{R}} \mathcal{A}(t)$ , where  $\mathcal{A}(t)$  is a compact subset of  $X$  at each time  $t$ . For each  $t \in \mathbb{R}$ , this family has two fundamental properties:

- (1) **Invariance:**  $\Phi(t, s)\mathcal{A}(s) = \mathcal{A}(t)$ , for all  $t \geq s$ , and
- (2) **Pullback attraction:** For any nonempty subset  $B$  of  $X$ ,

$$\lim_{s \rightarrow -\infty} d_X(\Phi(t, s)B, \mathcal{A}(t)) = 0,$$

where  $d_X$  is the Hausdorff semi-distance in  $X$ .

According to (1) and (2) above, the family  $\mathcal{A}(t)$  is invariant under the system's dynamics and it attracts at each time  $t$  all compact initial subsets  $B$  from the remote past; see also Ghil et al. [7, Fig. A.1] for a simple illustration.

## APPENDIX B: RANDOM DYNAMICAL SYSTEMS (RDS)

In physical systems, such as those encountered in the climate sciences, random time-dependent forcing is often present [4]. When that is so, it becomes necessary to model this type of systems using stochastic differential equations (SDEs) [6].

In the theory of RDSs, random PBAs are known as *random attractors* and they can be constructed in an extended phase space composed of the phase space  $X$  and a probability space associated with the paths of the driving noise. A probability space  $(\Omega, \mathcal{F}, \mathbb{P})$  is a three-tuple, where  $\Omega$  is the sample space;  $\mathcal{F}$  is the event space, formulated as a  $\sigma$ -algebra; and  $\mathbb{P}$  is a probability measure on  $\mathcal{F}$ ; see [6, Appendix A].

The probability space is then endowed with a time-dependent shift  $\theta_t$ . In the case of a stochastic-dynamic system driven by a Wiener process, as is the case here, this shift is defined on  $\Omega$  according to  $W_s(\theta_t \omega) = W_{t+s}(\omega) - W_s(\omega)$  [6]. With this mapping  $\theta_t$  in hand, the noise realization  $\omega$  evolves in time, and one can define a cocycle to describe the evolution of the state  $x$ .

A mapping  $\varphi : \mathbb{R} \times \Omega \times X \rightarrow X$  has the cocycle property when  $\varphi(t, \omega) = \varphi(t, \omega, \cdot) : X \rightarrow X$  satisfies the following conditions [6]:

- (i)  $\varphi(0, \omega)x = x$ , for all  $x \in X$  and  $\omega \in \Omega$ , and
- (ii)  $\varphi(t+s, \omega) = \varphi(t, \theta_s(\omega)) \circ \varphi(s, \omega)$ , for all  $s, t \in \mathbb{R}$  and  $\omega \in \Omega$ , where  $\circ$  denotes the composition operation for mappings of  $X$ .

Property (i) just sets the initial state of the cocycle, while property (ii) states that a cocycle is an expression of the existence and uniqueness of solutions, in the sense that going from a copy of  $X$  at time 0 to one at time  $s$  and from there on to one at time  $t+s$  is the same as going directly from 0 to  $t+s$ ; see also Ghil et al. [7, Fig. A.2]. This cocycle property is satisfied for a broad class of SDEs like those of interest here; see [6].

Mathematically, given an SDE with the right properties, the probability space  $(\Omega, \mathcal{F}, \mathbb{P})$  equipped with the collections of shifts  $\theta = \{\theta_t\}_{t \in \mathbb{R}}$ , and its associated cocycle  $\varphi$ , form what is called an RDS  $(\varphi, \theta)$ , also called sometimes an RDS  $\varphi$  over  $\theta$ .

The evolution of a stochastic-dynamic system can be thus modeled by an RDS and its associated random attractor  $\bigcup_{t \in \mathbb{R}} \mathcal{A}(t; \omega)$  can be seen as an extension of a

PBA, as defined in Appendix A. In the RDS case, however, each individual “random PBA” depends on the specific realization  $\omega \in \Omega$  of the noise. The resulting family of random compact sets  $\bigcup_{\omega \in \Omega} \mathcal{A}(\omega)$  provides a complete description of all the possible states of the system that are likely to be observed at time  $t$ .

### APPENDIX C: INVARIANT MEASURES

A number of interesting properties follow from the fact that the RDS  $(\theta, \varphi)$  has a random attractor. One of these is the existence of invariant measures of  $(\theta, \varphi)$ , in the sense of RDS theory. In this Appendix, we briefly clarify this notion and discuss the properties of these measures.

To do so, recall that any RDS  $(\theta, \varphi)$  generates a skew-product semiflow  $\{\Theta(t)\}_{t \geq 0}$  on  $\Omega \times X$  by the formula

$$\Theta(t)(\omega, x) = (\theta_t \omega, \varphi(t, \omega)x), \quad t \geq 0. \quad (3)$$

The cocycle property for  $\varphi$  is equivalent to the semigroup property for  $\Theta(t)$ , namely  $\Theta(t+s) = \Theta(t)\Theta(s)$ . In what follows we denote by  $\mathcal{B}$  the  $\sigma$ -algebra of Borel sets in  $X$ ; see [6]. We have then the following definition.

**Definition 2** *Given an RDS  $(\varphi, \theta)$ , a probability measure  $\mu$  on  $(\Omega \times X, \mathcal{F} \times \mathcal{B})$  is called an invariant measure for  $\varphi$  if it satisfies:*

- (i)  $\Theta(t)\mu = \mu$ , for all  $t \in \mathbb{R}$ .
- (ii) *The basic probability measure  $\mathbb{P}$  is the marginal on  $(\Omega, \mathcal{F})$  of  $\mu$ , i.e.  $\mu(E \times X) = \mathbb{P}(E)$  for any  $E \in \mathcal{F}$ .*

It is known that any probability measure  $\mu$  on  $(\Omega \times X, \mathcal{F} \times \mathcal{B})$  possesses a *disintegration* or factorization [6], given by a function  $(\omega, B) \mapsto \mu_\omega(B)$  from  $\Omega \times \mathcal{B}$  into the interval  $[0, 1]$  such that:

- (i) For any  $B \in \mathcal{B}$ ,  $\mu_\omega$  is  $\mathcal{F}$ -measurable;
- (ii) there exists a measurable set  $\Omega'$  in  $\Omega$  such that  $\mathbb{P}(\Omega') = 1$  and  $\mu_\omega$  is a probability measure on  $(X, \mathcal{B})$  for all  $\omega$  in  $\Omega'$ ; and

(iii) for all  $f$  in  $L^1_\mu(\Omega \times X)$  we have

$$\int_{\Omega \times X} f(\omega, x) \mu(d\omega, dx) = \int_{\Omega} \left( \int_X f(\omega, x) \mu_\omega(dx) \right) \mathbb{P}(d\omega). \quad (4)$$

The disintegration  $\mu_\omega$  is unique  $\mathbb{P}$ -almost surely and it is also called a *sample measure* [41]. The invariance property (i) of Definition 2 translates into  $\varphi(t, \omega)\mu_\omega = \mu_{\theta_t \omega}$ , in terms of sample measures.

When an RDS  $(\theta, \varphi)$  possesses a random compact attractor, then it supports every invariant measure, i.e.  $\mu_\omega(\mathcal{A}(\omega)) = 1$  for almost all  $\omega$  in  $\Omega$ . In this case, the sample measure possesses a useful interpretation. To understand it, recall that, roughly speaking, the random attractor  $\mathcal{A}(t; \omega)$  determines the portions of the phase space  $X$  onto which any bounded set  $B$  is mapped at time  $t$ , when  $B$  is propagated by the cocycle  $\varphi$  from a remote past. The sample measure  $\mu_{\theta_t \omega}$  supported by the random attractor  $\mathcal{A}(t; \omega)$  provides, therewith, the spatio-temporal probability distributions of the portions of the phase space  $X$  “selected” by the RDS.

*Physical measures* are sample measures of special interest [4, 13]. A closely related class of sample measures is that of Sinai-Ruelle-Bowen (SRB) measures [12, 40, 41]. Chekroun et al. [13, Appendix C] have proven rigorously that LORA supports an SRB measure when its generator (1) is in a chaotic regime, and provided strong numerical evidence that it must be physical, too.

For clarity, recall that an SRB measure  $\mu$  — subject to certain technical conditions — is physical in the following, more precise sense; namely, that for any continuous observable  $\psi : X \rightarrow \mathbb{R}$ , the time average equals the ensemble average for almost all initial data  $x_0$ , with respect to the usual, Lebesgue measure, where  $x_0 \in B_\mu$  and  $B_\mu$  is the basin of attraction of  $\mu$ ; see Chekroun et al. [13, Eq. (5)]. A technical condition is that the linearization of the cocycle  $\varphi(t, \omega, x)$  at  $x$  must have a positive Lyapunov exponent for  $\mu$ -almost every  $x$ ; this condition implies that the system is chaotic. For the other sufficient conditions, please see Chekroun et al. [13, Appendix C].

Note that the existence of an SRB measure  $\mu$  does not guarantee its uniqueness, and that two such measures  $\mu \neq \nu$  may also have different attractor sets  $B_\mu \neq B_\nu$ . The extensive numerical calculations in [13] and herein have given no indication, though, of another SRB measure being present. Still, the uniqueness of LORA’s SRB, and hence physical, measure has not been proven rigorously, to the best of the authors’ knowledge.

---

[1] M. Ghil and S. Childress, *Topics in Geophysical Fluid Dynamics: Atmospheric Dynamics, Dynamo Theory, and Climate Dynamics* (Springer, 1987, reissued, 2012).  
[2] C.-P. Chang et al., *Climate Change: Multidecadal and Beyond* (World Scientific, 2015).  
[3] M. Ghil, *Earth and Space Science* **6**, 1007 (2019).

[4] M. Ghil and V. Lucarini, *Rev. Mod. Phys.* **92**, 035002 (2020).  
[5] P. E. Kloeden and M. Rasmussen, *Nonautonomous Dynamical Systems* (American Meteorological Society, 2011).  
[6] L. Arnold, *Random Dynamical Systems* (Springer, 1988).

- [7] M. Ghil, M. D. Chekroun, and E. Simonnet, *Phys. D* **237**, 2111 (2008).
- [8] M. Gladwell, *The Tipping Point: How Little Things Can Make a Big Difference* (Little, Brown, 2006).
- [9] T. M. Lenton et al., *Proc. Natl. Acad. Sci. USA* **105**, 1786 (2008).
- [10] M. D. Chekroun, M. Ghil, and J. D. Neelin, in *Adv. Nonlin. Geophys.*, edited by A. Tsonis (Springer Science & Business Media, 2018), pp. 1–33.
- [11] F. Ledrappier and L.-S. Young, *Probab. Theory Related Fields* **80**, 217 (1988).
- [12] L.-S. Young, *J. Stat. Phys.* **166**, 494 (2017).
- [13] M. D. Chekroun, E. Simonnet, and M. Ghil, *Phys. D* **240**, 1685 (2011).
- [14] H. Poincaré, *J. Èc. polythec. Mat.* **1**, 1 (1985).
- [15] A. Hatcher, *Algebraic Topology* (Cambridge University Press, 2002).
- [16] G. M. Mindlin and R. Gilmore, *Phys. D* **58**, 229 (1992).
- [17] R. Gilmore, *Rev. Mod. Phys.* **4**, 1455 (1998).
- [18] M. R. Muldoon et al., *Phys. D* **65**, 1 (1993).
- [19] J. Birman and R. F. Williams, *Topology* **22**, 47 (1983).
- [20] P. Holmes and R. F. Williams, *Arch. Ratio. Mech. Anal.* **90**, 115 (1985).
- [21] D. Sciamarella and G. B. Mindlin, *Phys. Rev. E* **64**, 036209 (2001).
- [22] D. Sciamarella and G. B. Mindlin, *Phys. Rev. Lett.* **82**, 1450 (1999).
- [23] G. D. Charó, G. Artana, and D. Sciamarella, *Phys. D* **405**, 132371 (2020).
- [24] L. C. Kinsey, *Topology of Surfaces* (Springer, 1997).
- [25] F. Chazal and M. Bertrand, arXiv:1710.04019 (2017).
- [26] L. Wasserman, *Annu. Rev. Stat. Appl.* **5**, 501 (2018).
- [27] J. Murugan and D. Robertson, arXiv:1904.11044 (2019).
- [28] G. Carlsson et al., *Int. J. Comput. Vis.* **76**, 1 (2008).
- [29] D. Taylor et al., *Nat. Commun.* **6**, 1 (2015).
- [30] L. Speidel et al., *Phys. Rev. E* **98**, 012318 (2018).
- [31] J. M. Chan, G. Carlsson, and R. Rabadan, *Proc. Natl. Acad. Sci. USA* **110**, 18566 (2013).
- [32] R. Rabadan and A. Blumberg, *Topological Data Analysis for Genomics and Evolution: Topology in Biology* (Cambridge: Cambridge University Press, 2019).
- [33] M. Gameiro et al., *Jpn J. Ind. Appl. Math.* **32**, 1 (2015).
- [34] H. Edelsbrunner and J. Harer, *Contemp. Math.* **453**, 257 (2008).
- [35] G. Carlsson, *Acta Num.* **23**, 289 (2014).
- [36] S. Maletić, Y. Zhao, and M. Rajković, *Chaos* **26**, 053105 (2016).
- [37] E. N. Lorenz, *J. Atmos. Sci.* **20**, 130 (1963).
- [38] F. J. Romeiras, C. Grebogi, and E. Ott, *Phys. Rev. A* **41**, 784 (1990).
- [39] G. Drótos, T. Bódai, and T. Tél, *J. Climate* **28**, 3275 (2015).
- [40] J.-P. Eckmann and D. Ruelle, *Rev. Mod. Phys.* **57**, 617 (1985).
- [41] L.-S. Young, *J. Stat. Phys.* **108**, 733 (2002).
- [42] T. Caravallo, G. Łukaszewicz, and J. Real, *Nonlinear Anal.* **64**, 484 (2006).
- [43] M. D. Chekroun, M. Ghil, and J. D. Neelin, in *Advances in Nonlinear Geosciences*, edited by A. A. Tsonis (Springer Science & Business Media, 2018), pp. 1–33.